Journal of Sound and Vibration (1998) **212**(3), 525–546

CRITICAL SEISMIC VECTOR RANDOM EXCITATIONS FOR MULTIPLY SUPPORTED STRUCTURES

A. Sarkar

Department of Engineering Science, University of Oxford, Parks Road, Oxford OX1 3PJ, England

AND

C. S. Manohar

Department of Civil Engineering, Indian Institute of Science, Bangalore 560012, *India*

(*Received* 1 *May* 1997, *and in final form* 12 *December* 1997)

A method for determining critical power spectral density matrix models for earthquake excitations which maximize steady response variance of linear multiply supported extended structures and which also satisfy constraints on input variance, zero crossing rates, frequency content and transmission time lag has been developed. The optimization problem is shown to be non-linear in nature and solutions are obtained by using an iterative technique which is based on linear programming method. A constraint on entropy rate as a measure of uncertainty which can be expected in realistic earthquake ground motions is proposed which makes the critical excitations more realistic. Two special cases are also considered. Firstly, when knowledge of autospectral densities is available, the critical response is shown to be produced by fully coherent excitations which are neither in-phase nor out-of-phase. The critical phase between the excitation components depends on structural parameters, but independent of the auto-spectral densities of the excitations. Secondly, when the knowledge of autospectral densities and phase spectrum of the excitations is available, the critical response is shown to be produced by a system dependent coherence function representing neither fully coherent nor fully incoherent ground motions. The applications of these special cases are discussed in the context of land-based extended structures and secondary systems such as nuclear piping assembly. Illustrative examples on critical inputs and response of sdof and a long-span suspended cable which demonstrated the various features of the approach developed are presented.

1. INTRODUCTION

Design earthquake ground motions for engineering structures are specified in terms of time histories, response spectra or random processes which typically include the definition of a deterministic envelope and a psd function [1]. These three methods of seismic load specification are not mutually independent in the sense that exchange of one form of specification compatible with any other is possible. The accuracy and robustness of these seismic input models are open to question in view of significant uncertainties which are present in the earthquake excitation mechanism on the one hand, and the scarcity of the data on the other. Given this ill-posed nature of the problem, it is natural to ask what is the worst that might happen to a given structure under a set of incompletely specified seismic loading conditions. The method of critical excitations has been developed to answer this question, these excitations being defined as those which produce the highest

0022–460X/98/180525 + 22 $25.00/0/sv971460

damage to a given structure and at the same time satisfy a set of constraints reflecting some of the well known features of earthquake time histories. Thus, the critical excitations, by definition, depend upon the system under consideration, nature of partial information available and the damage variable chosen for optimization and their determination constitutes an inverse problem in structural dynamics.

In the past, critical excitations have been derived for all the three forms of seismic load specifications, namely, time histories [2–6], response spectra [4, 5, 7, 8] and random process models [7, 9–12]. In recent work the authors [11] considered non-stationary Gaussian random process models for critical excitations. The systems considered are linear single-degree-of-freedom (sdof) or multi-degree-of-freedom (mdof) systems, and the damage variable chosen is the highest response variance. The excitations are constrained to have a given non-stationarity trend, duration, frequency content, total average energy and average zero crossing rate. The variable of optimization is the power spectral density (psd) function of the stationary component of the excitation and the problem is solved with the framework of linear programming. The critical excitations conforming to this definition have been shown to be strongly resonant and narrow-banded. This clearly indicates a major shortcoming in the definition of the critical excitations in the sense that they fail to capture the random nature of the recorded accelerograms. To overcome this limitation, we have proposed that the entropy rate of the ground acceleration process be considered as a quantitative measure of randomness in seismic loads and that it be considered as an additional constraint in the definition of critical excitation.

A notable feature of the existing literature on critical excitations has been the fact that in all the studies seismic loads have been considered as single point excitations: that is, the same excitation is assumed to act at all the supports. This assumption becomes questionable if interest is focused on extended land-based structures such as long-span bridges, pipelines, dams and power transmission systems or multiply supported secondary systems such as pipings in nuclear power installations. In the case of land-based extended structures, the supports can be expected to suffer differential ground motions which are caused due to phase lag and coherency loss effects. Spurred by the availability of densely spaced seismic array data, several studies have been conducted in the recent past on the effects of spatial variability and wave propagation on the earthquake responses of large or multiply supported structures [13–21]. A detailed theoretical treatment of modeling the coherency function for spatially varying ground motion has been presented by Der Kiureghian [22]. A comprehensive review of the relevant issues can be found in the recent paper by Banerjee [23].

The present study is concerned with the extension of methods developed in reference [11] to the problem of determination of critical vector random process models for earthquake loads acting on extended structures supported discretely at two points. The excitation here is modelled as a partially specified stationary vector Gaussian random process with a given variance, frequency content and average zero crossing rate and an unknown psd matrix. The input psd matrix is found such that the steady state response variance of a given linear system is maximized. It turns out that the optimization problem in this case becomes non-linear in nature, which is in contrast with the critical single point excitation problem, wherein the problem remains linear [11]. In this study, an iterative method of nonlinear optimization which converts the problem at every iteration into a linear programming problem is developed. Two special cases which would arise if the knowledge of the autospectral density functions is available but the knowledge of the cross-power spectrum is lacking are also considered. Specifically, when the autospectra are known and the wave passage effect is explicitly modelled through a known phase spectrum, it is shown that it is neither the fully coherent nor the fully incoherent excitations which

produce the highest response: instead, there exists a special form of cross-spectral density function which produces the highest response. This cross-spectrum is determined in terms of the system characteristics, damage variable and the known autospectral densities. The question of developing optimally disordered critical excitations by the use of entropy rate considerations is also discussed. A computational scheme which incorporates entropy rates as measures of disorder and enables the solution within the framework of iterative linear programming method is outlined. Illustrative examples on single-degee-of-freedom systems and a 1620 m suspended cable are presented.

2. MULTI-SUPPORT EXCITATIONS

2.1. INPUT PROCESSES

In Figure 1 is shown a sdof system supported at two points and subjected to support accelerations $\ddot{x}$ and $\ddot{y}$ which are modelled as a pair of stationary Gaussian band-limited random processes with psd matrix given

$$S(\omega) = \begin{pmatrix} S_{xx}(\omega) & S_{xy}(\omega) \\ S_{yx}(\omega) & S_{yy}(\omega) \end{pmatrix}. \tag{1}$$

The diagonal terms in this matrix represent the auto-psd functions while the off-diagonal terms are the cross-psd functions. The latter functions are in general complex valued and can be represented as

$$S_{xy}(\omega) = |S_{xy}(\omega)| \exp[-\mathrm{i}\phi_{xy}(\omega)]. \tag{2}$$

Alternatively, the function can be normalized with respect to the auto-psd functions which leads to the definition of the coherency function given by

$$\gamma_{xy}(\omega) = S_{xy}(\omega)/\sqrt{S_{xx}(\omega)S_{yy}(\omega)}. \tag{3}$$

It can be shown that $0 \leqslant |\gamma_{xy}(\omega)| \leqslant 1$, with $|\gamma_{xy}(\omega)| = 0$ representing the case of complete lack of linear dependence, which, for Gaussian random processes, also implies statistical independence and, $|\gamma_{xy}(\omega)| = 1$ denoting the condition for the two processes to be linearly dependent. Several features of spatial variability of earthquake ground motion get reflected through $|\gamma_{xy}(\omega)|$ and $\phi_{xy}(\omega)$; these include the incoherence effect, wave-passage effect and the site-response effect. The incoherence effect arises due to loss of statistical dependence of the ground motion at different points from scattering of waves in heterogeneous ground medium and differential superpositions of the waves arriving from extended source. The wave passage effect is due to the transmission time lag of the seismic wave propagation at different locations. The varying local soil conditions give rise to the site response effect. The wave passage and the site response effects give rise only to phase lag in the ground motions at different locations. The incoherence and wave passage effects are usually significant for long-span flexible structures, whereas the site-response

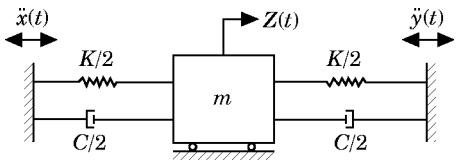

Figure 1. An sdof system with double support excitations.

effect is important for short-span stiff structures situated in the regions of varying soil properties [22]. Several models for $|\gamma_{xy}(\omega)|$ and $\phi_{xy}(\omega)$ have proposed in the existing literature based on recorded earthquake data [19–21, 23] and also based on theoretical considerations [22]. In many of the studies reported in the literature so far, the phase spectrum is taken to be of the form

$$\phi_{xy}(\omega) = \omega\tau, \tag{4}$$

where $\tau = L/V$ is the seismic transmission time lag over a span L with an apparent velocity of propagation V. This model for the phase spectrum is based on the assumption that (a) the phase differences arise due to the wave passage effect caused due to plane waves arriving at a single incident angle at the two stations, and (b) the contributions to the phase due to the differences in local soil conditions is considered negligible. This assumption is considered acceptable for modelling earthquake inputs to long-span structures [13, 14, 22].

2.2. RESPONSE OF SDOF SYSTEM

With reference to Figure 1, the governing equation of motion for the total displacement $z_t(t)$ is

$$m\ddot{z}_t + c\left\{\dot{z}_t - \frac{\dot{x}+\dot{y}}{2}\right\} + k\left\{z_t - \frac{x+y}{2}\right\} = 0. \tag{5}$$

In terms of the dynamic displacement $z = z_t - \frac{1}{2}(x+y)$ one obtains

$$\ddot{z} + 2\eta\omega_n\dot{z} + \omega_n^2 z = -\tfrac{1}{2}(\ddot{x}+\ddot{y}) \tag{6}$$

Let the force F in the left spring be considered as the response variable of interest. This is proportional to the relative displacement between the mass and the left support. The steady state variance of the quantity $4F/K$ can be shown to be given by

$$\sigma^2 = \int_{\omega_1}^{\omega_2} \{S_{xx}(\omega)H_1(\omega) + S_{yy}(\omega)H_2(\omega) + |S_{xy}(\omega)|H_3(\omega)\}\,\mathrm{d}\omega. \tag{7}$$

Here (ω_1, ω_2) is the frequency bandwidth and the transfer functions H_1, H_2 and H_3 are given by

$$H_1(\omega) = \left\{\frac{1}{\omega^4} + \frac{1}{(\omega^2-\omega_0^2)^2 + (2\eta\omega\omega_0)^2} + \frac{2(\omega^2-\omega_0^2)}{\omega^2[(\omega^2-\omega_0^2)^2 + (2\eta\omega\omega_0)^2]}\right\}|H_f(\omega)|^2, \tag{8}$$

$$H_2(\omega) = \left\{\frac{1}{\omega^4} + \frac{1}{(\omega^2-\omega_0^2)^2 + (2\eta\omega\omega_0)^2} - \frac{2(\omega^2-\omega_0^2)}{\omega^2[(\omega^2-\omega_0^2)^2 + (2\eta\omega\omega_0)^2]}\right\}|H_f(\omega)|^2, \tag{9}$$

$$H_3(\omega) = \left\{\frac{-2\cos[\phi_{xy}(\omega)]}{\omega^4} + \frac{2\cos[\phi_{xy}(\omega)]}{(\omega^2-\omega_0^2)^2 + (2\eta\omega\omega_0)^2} + \frac{8\eta\omega\omega_0\sin[\phi_{xy}(\omega)]}{\omega^2[(\omega^2-\omega_0^2)^2 + (2\eta\omega\omega_0)^2]}\right\}|H_f(\omega)|^2. \tag{10}$$

The filter function $H_f(\omega)$ appearing in these equations is given by

$$|H_f(\omega)|^2 = \frac{(\omega/\omega_f)^4}{[1-(\omega/\omega_f)^2]^2 + [4\zeta_f^2(\omega/\omega_f)^2]}, \tag{11}$$

this being an artifact to remove the singularity in the support displacement at $\omega = 0$ which would otherwise be present [24]. It may be noted that the functions H_1 and H_2 can also be written in the forms

$$H_1(\omega) = \frac{(2\omega^2 - \omega_0^2)^2 + (2\eta\omega\omega_0)^2}{\omega^4[(\omega^2 - \omega_0^2)^2 + (2\eta\omega\omega_0)^2]} |H_f(\omega)|^2, \tag{12}$$

and

$$H_2(\omega) = \frac{\omega_0^2(\omega_0^2 + 4\eta^2\omega^2)}{\omega^4[(\omega^2 - \omega_0^2)^2 + (2\eta\omega\omega_0)^2]} |H_f(\omega)|^2, \tag{13}$$

from which it follows that the functions H_1 and H_2 are non-negative. It can however be noted that, depending on the value of $\phi_{xy}(\omega)$, $H_3(\omega)$ can take either negative or positive values.

2.3. RESPONSE OF SUSPENDED CABLE STRUCTURE

The formulation presented above can be easily extended to mdof systems. For a structure with two supports, the expression for the steady state response variance at any point α_0 can again be expressed in the form of equation (7). The expressions for the generalized transfer functions H_1, H_2 and H_3 will now be also dependent on α_0. For the purpose of illustration consider a damped cable element shown in Figure 2. The dynamic stiffness coefficient $D_{ij}(\omega)$, $i, j = 1, \ldots, 4$, is defined as the amplitude of harmonic force at node j due to a harmonic displacement of unit amplitude and frequency ω at node i with all other nodes being held fixed [24]. For a damped cable element, these coefficients are complex in nature and consequently, it is useful to separate the real and imaginary parts of nodal displacements and forces as shown in Figure 2. In this figure, the Δ's represent displacements, the p's the forces and the subscripts R and I denote, respectively, the real and imaginary parts. Introducing a displacement vector Δ and a force vector P defined, respectively, by

$$\begin{aligned} \Delta^* &= [\Delta_{R1}, \Delta_{I1}, \Delta_{R2}, \Delta_{I2}, \Delta_{R3}, \Delta_{I3}, \Delta_{R4}, \Delta_{I4}] \\ p^* &= [p_{R1}, p_{I1}, p_{R2}, p_{I2}, p_{R3}, p_{I3}, p_{R4}, p_{I4}], \end{aligned} \tag{14}$$

where the asterisk denotes matrix transposition, one can define a generalized dynamic stiffness matrix K of size 8×8 which relates the vectors Δ and p through the relation

$$p = K\Delta. \tag{15}$$

The elements K_{ij}, $i, j = 1, \ldots 8$, are all real and can be evaluated either in terms of the system eigensolutions or, alternatively, by direct integration in space of an associated set

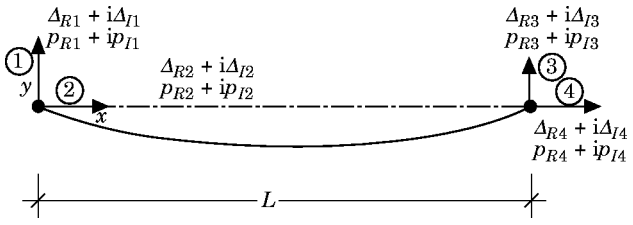

Figure 2. A cable element.

of boundary value problems. In this study, we take the latter approach and compute the stiffness coefficients using a numerical integration scheme detailed elsewhere [28].

Two cases are now considered: firstly, when the seismic excitations act in the vertical direction, that is along directions 1 and 3, and the damage variable of interest be the steady state variance of vertical force transmitted to the left end support, and, secondly, let the excitations be along directions 2 and 4 and the response variable of interest be the horizontal component of the force transmitted to the left support. In both these cases, the response variance can again be expressed in the form of equation (7). The expressions for H_1, H_2 and H_3 differ for each case. Thus, for the first case it can be shown that

$$H_1 = \frac{|H_f(\omega)|^2}{\omega^4}[K_{11}^2 + K_{12}^2], \qquad H_2 = \frac{|H_f(\omega)|^2}{\omega^4}[K_{15}^2 + K_{16}^2],$$

$$H_3 = \frac{2|H_f(\omega)|^2}{\omega^4}\{\cos[\phi_{xy}(\omega)](K_{11}K_{15} + K_{12}K_{16}) - \sin[\phi_{xy}(\omega)](K_{11}K_{16} - K_{12}K_{15})\}, \quad (16)$$

and, similarly, for the second case,

$$H_1 = \frac{|H_f(\omega)|^2}{\omega^4}[K_{31}^2 + K_{32}^2], \qquad H_2 = \frac{|H_f(\omega)|^2}{\omega^4}[K_{35}^2 + K_{36}^2],$$

$$H_3 = \frac{2|H_f(\omega)|^2}{\omega^4}\{\cos[\phi_{xy}(\omega)](K_{31}K_{35} + K_{32}K_{36}) + \sin[\phi_{xy}(\omega)](K_{31}K_{36} - K_{32}K_{35})\}, \quad (17)$$

Again, notice that $H_1(\omega)$ and $H_2(\omega)$ are always non-negative, while $H_3(\omega)$ can take either negative or positive values. As has been already noted, the critical psd matrix depends upon the system properties and this dependence, as will be shown in the next section, is pivoted on the nature of the functions $H_1(\omega)$, $H_2(\omega)$ and $H_3(\omega)$.

3. CRITICAL INPUT PSD MATRIX

As has been pointed out in the introduction, critical excitations, by definition, are dependent on the system properties, damage variable chosen for maximization and the constraints imposed on the class of allowable inputs. We consider three classes of problems: (A) to find the critical $|S_{xy}(\omega)|$ and $\phi_{xy}(\omega)$ given the knowledge of $S_{xx}(\omega)$ and $S_{yy}(\omega)$; (B) to find the critical $|S_{xy}(\omega)|$ given the knowledge of $S_{xx}(\omega)$, $S_{yy}(\omega)$ and $\phi_{xy}(\omega)$; (C) to find the critical $|S_{xy}(\omega)|$, $S_{xx}(\omega)$ and $S_{yy}(\omega)$ given the knowledge of $\phi_{xy}(\omega)$.

3.1. CASE (A): CRITICAL CROSS-PSD FUNCTION GIVEN AUTO-PSD FUNCTIONS

Here we consider the special case in which the knowledge for $S_{xx}(\omega)$ and $S_{yy}(\omega)$ is available, while $|S_{xy}(\omega)|$ and $\phi_{xy}(\omega)$ are unknown functions. This situation can be easily conceived, since information from densely spaced seismic arrays is more scarce than data from single point ground acceleration measurements. In this case, the problem of critical excitations consists of findings $|S_{xy}(\omega)|$ and $\phi_{xy}(\omega)$ which maximize σ^2 as given by equation (7) under the constraint that $0 \leqslant |S_{xy}(\omega)| \leqslant \sqrt{S_{xx}(\omega)S_{yy}(\omega)}$. It can be easily observed from equation (7) that the contribution from the third term in the integrand at any frequency ω can be either positive or negative depending on the sign of the function $H_3(\omega)$. We re-write the function $H_3(\omega)$ as

$$H_3(\omega) = R(\omega)\cos[\phi_{xy}(\omega) - \alpha(\omega)], \quad (18)$$

where

$$R(\omega) = \sqrt{[g_1^2(\omega) + g_2^2(\omega)]}, \qquad \alpha(\omega) = \tan^{-1}\{g_2(\omega)/g_1(\omega)\},$$

$$g_1(\omega) = \left\{\frac{-2}{\omega^4} + \frac{2}{(\omega^2 - \omega_0^2)^2 + (2\eta\omega\omega_0)^2}\right\}|H_f(\omega)|^2,$$

$$g_2(\omega) = \left\{\frac{8\eta\omega\omega_0}{\omega^2[(\omega^2 - \omega_0^2)^2 + (2\eta\omega\omega_0)^2]}\right\}|H_f(\omega)|^2. \tag{19}$$

It clearly follows that, for σ^2 to be the maximum, it is required that

$$|S_{xy}| = \sqrt{S_{xx}\,S_{yy}} \qquad \text{and} \qquad \cos(\phi - \alpha) = 1. \tag{20}$$

This would mean that

$$\phi_{xy}(\omega) = \alpha(\omega) = \tan^{-1}\{g_2(\omega)/g_1(\omega)\}. \tag{21}$$

Similarly, it is of interest to note that the *least* response is produced when

$$|S_{xy}| = \sqrt{S_{xx}\,S_{yy}} \qquad \text{and} \qquad \cos(\phi - \alpha) = -1, \tag{22}$$

which, in turn, means

$$\phi_{xy}(\omega) = \pi + \alpha(\omega) = \pi + \tan^{-1}\{g_2(\omega)/g_1(\omega)\}. \tag{23}$$

It thus follows that the highest and lowest response are produced by coherent motions ($|\gamma_{xy}(\omega)| = 1$), but the phase spectrum differs for the two cases. It is also evident that the critical responses are produced by neither in-phase nor out-of-phase motions. The critical $\phi_{xy}(\omega)$ is a non-linear function of frequency ω and system parameters ω_0 and η and does not depend on $S_{xx}(\omega)$ and $S_{yy}(\omega)$. This model of the critical $S_{xy}(\omega)$ may be suitable for ground motions where the spatial variability is mainly dominated by the site-response effect, the information about which is considered unknown. This essentially implies that this model can be used to study the critical response of short-span structures founded on rapidly varying local soil conditions.

This model is also suitable for studying the response bounds of secondary structures such as piping assembly in nuclear power plants subject to multi-support seismic excitations. In the current analysis and design procedures, the support inputs of a piping system supported at different locations in the primary structure are specified in terms of floor response spectra. Since the floor response spectra do not contain any phasing information of the different support motions, various approximate techniques are used to obtain conservative estimates of the response to compensate for the phase information neglected in the analysis [30]. The conservatism obtained by these approximate methods is neither uniform nor assured. In this situation, the present formulation, being exact in producing the upper bound of the response, can be used to study the validity and rationale of the existing design practice.

3.2. CASE (B): CRITICAL CROSS-PSD FUNCTION GIVEN AUTO-PSD FUNCTIONS AND PHASE SPECTRUM

In this case we assume that the prior knowledge about the input is available not only on the auto-psd functions but also on the phase spectrum $\phi_{xy}(\omega)$. Specifically, we take the phase spectrum to be as given in equation (4). This case is considered relevant to problems in which the major contribution to $\phi_{xy}(\omega)$ comes from the wave passage effect which can be reasonably modelled through the time lag τ, such as long-span structures

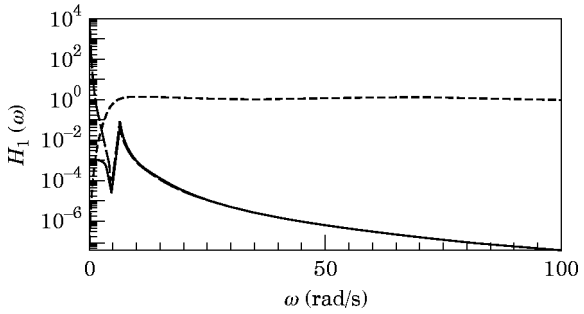

Figure 3. Transfer function H_1 for an sdof system; $\omega_n = 6{\cdot}1$ rad/s, $\eta = 0{\cdot}05$. ——, Filter included; ----, filters— —, filter excluded.

[22]. Here information about the coherency loss of the excitations is taken to be unknown. In this case, the problem of critical excitations consists of finding $|S_{xy}(\omega)|$ which maximizes σ^2 as given by equation (7) under the constraint that $0 \leqslant |S_{xy}(\omega)| \leqslant \sqrt{S_{xx}(\omega)S_{yy}(\omega)}$. Again, it may be observed from equation (7) that the contribution from the third term in the integrand at any frequency ω can be either positive or negative depending on the sign of the function $H_3(\omega, \tau)$. Consequently, it can be easily deduced that the optimal $|S_{xy}(\omega)|$ which produces the highest response variance must be of the form

$$|S_{xy}(\omega)| = 0 \quad \text{if} \quad H_3(\omega, \tau) < 0,$$
$$|S_{xy}(\omega)| = \sqrt{S_{xx}(\omega)S_{yy}(\omega)} \quad \text{if} \quad H_3(\omega, \tau) > 0. \tag{24}$$

Thus, the critical cross-psd depends upon the transfer function $H_3(\omega, \tau)$, $S_{xx}(\omega)$ and $S_{yy}(\omega)$ and the highest response occurs neither when $\ddot{x}(t)$ and $\ddot{y}(t)$ are fully coherent nor when they are fully incoherent but, instead, when the two processes have the specific correlation properties as given above. This special class of problems has been recently discussed in greater detail in the authors' recent paper [29], in which structures with more than two supports and also presence of multi-component excitations have been studied.

3.3. CASE (C): CRITICAL AUTO- AND CROSS-PSD FUNCTIONS GIVEN PHASE SPECTRUM

Here we consider the more general case when $S_{xx}(\omega)$, $S_{yy}(\omega)$ and $|S_{xy}(\omega)|$ are unknown while it is assumed that the variance and the average zero crossing rate of the processes

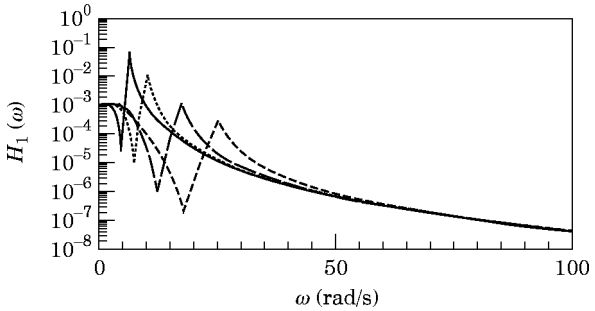

Figure 4. Transfer function H_1 for an sdof system; $\eta = 0{\cdot}05$. Natural frequency (rad/s): ——, 6·1; ·····, 10·0; — —, 17·0; ----, 25·1.

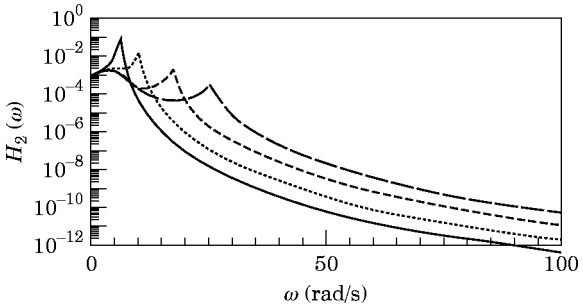

Figure 5. Transfer function H_2 for sdof systems; $\eta = 0{\cdot}05$. Key as Figure 4.

$\ddot{x}(t)$ and $\ddot{y}(t)$ are known. That is, the knowledge of E_{0x}, E_{0y}, n_{0x}^+ and n_{0y}^+, given, respectively, by

$$E_{0x} = \int_{\omega_1}^{\omega_2} S_{xx}(\omega)\,\mathrm{d}\omega, \qquad E_{0y} = \int_{\omega_1}^{\omega_2} S_{yy}(\omega)\,\mathrm{d}\omega,$$

$$n_{0x}^+ = E_{2x}/2\pi E_{0x}, \qquad n_{0y}^+ = E_{2y}/2\pi E_{0y}, \tag{25}$$

is taken to be available. Here, E_{2x} and E_{2y} are given by

$$E_{2x} = \int_{\omega_1}^{\omega_2} \omega^2 S_{xx}(\omega)\,\mathrm{d}\omega, \qquad E_{2y} = \int_{\omega_1}^{\omega_2} \omega^2 S_{yy}(\omega)\,\mathrm{d}\omega. \tag{26}$$

Additionally, it is assumed that $\phi_{xy}(\omega)$ is as given by equation (4). From equations (25) and (26) it is clear that the knowledge of variance and average zero crossing rate essentially implies the knowledge of the zeroth and second spectral moments of $S_{xx}(\omega)$ and $S_{yy}(\omega)$. The critical psd matrix is defined as the $S(\omega)$ which maximize σ^2 given by equation (7) under the constraints of equations (25) and (26) and the additional constraint

$$0 \leqslant |S_{xy}(\omega)| \leqslant \sqrt{S_{xx}(\omega) S_{yy}(\omega)}. \tag{27}$$

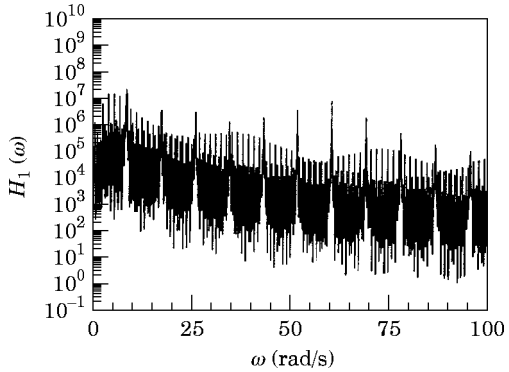

Figure 6. Transfer function H_1 for the vertical force transmitted to the left support for the 1620 m span cable with vertical support motions.

To solve this optimization problem, we first discretize the psd functions as follows:

$$S_{xx}(\omega) = \sum_{n=1}^{N} a_n \, \delta(\omega - \lambda_n), \qquad S_{yy}(\omega) = \sum_{n=1}^{N} b_n \, \delta(\omega - \lambda_n),$$

$$|S_{xy}(\omega)| = \sum_{n=1}^{N} c_n \, \delta(\omega - \lambda_n), \tag{28}$$

where $\delta(\cdot)$ is the Dirac delta function and $\lambda_n = n\lambda_0$.

It may be noted that this scheme of discretization of the psd functions is similar to the one followed in digital simulation of random processes when using Fourier series representations [1]. The optimization problem can now be stated as to find a_n, b_n and c_n which maximize

$$\sigma^2 = \sum_{n=1}^{N} a_n H_1(\lambda_n) + b_n H_2(\lambda_n) + c_n H_3(\lambda_n, \tau), \tag{29}$$

under the constraints

$$E_{0x} = \sum_{n=1}^{N} a_n, \qquad E_{0y} = \sum_{n=1}^{N} b_n, \qquad E_{2x} = \sum_{n=1}^{N} \lambda_n^2 a_n, \qquad E_{2y} = \sum_{n=1}^{N} \lambda_n^2 b_n, \tag{30}$$

$$a_n \geqslant 0, \qquad b_n \geqslant 0, \qquad c_n \geqslant 0, \tag{31}$$

$$c_n^2 \leqslant a_n b_n, \qquad n = 1, 2, \ldots, N. \tag{32}$$

Notice that the objective function, and all the contraints except the inequalities $c_n^2 \leqslant a_n b_n$, are linear functions of a_n, b_n and c_n. The problem is, therefore, non-linear in nature. Furthermore, it can also be shown that the problem is non-convex in nature. The solution of this problem is proposed to be sought by using the method of approximate programming which is an iterative method based on the use of linear programming [25]. This consists of linearizing the non-linear constraints about a feasible starting solution and solving the resulting linear problem by using the linear programming method. Thus, at the jth step, the problem is to find $a_{j+1,n}$, $b_{j+1,n}$ and $c_{j+1,n}$ which maximize

$$\sigma_j^2 = \sum_{n=1}^{N} a_{j+1,n} H_1(\lambda_n) + b_{j+1,n} H_2(\lambda_n) + c_{j+1,n} H_3(\lambda_n, \tau) \tag{33}$$

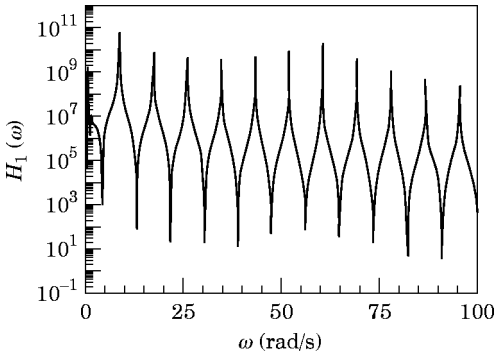

Figure 7. Transfer function H_1 for the horizontal force transmitted to the left support for the 1620 m span cable with horizontal support motions.

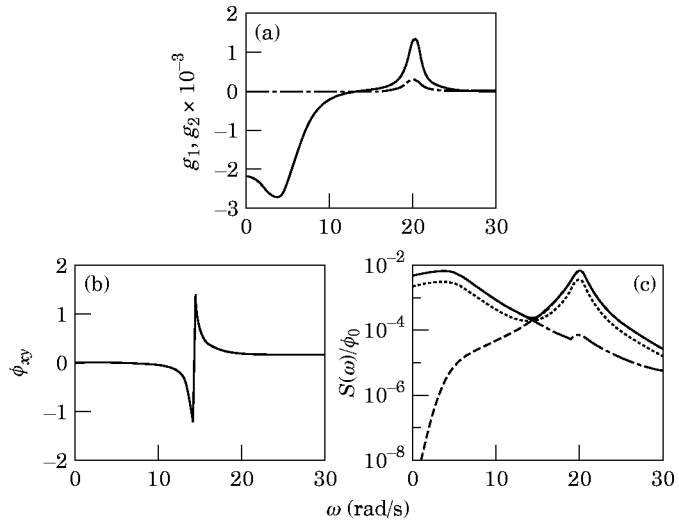

Figure 8. (a) g_1 (——) and g_2 (–·–·–) for $\omega_n = 20$ rad/s, $\eta = 0{\cdot}05$; (b) critical ϕ_{xy} for $\omega_n = 20$ rad/s. $\eta = 0{\cdot}05$ and (c) response psd of $4F/K$ for different cases of fully coherent ground motions in (1) critical phase (—), (2) in-phase (----), (3) out-of-phase (–·–·–) and (4) independent (· · · · · · ·) motions.

under the constraints

$$E_{0x} = \sum_{n=1}^{N} a_{j+1,n}, \qquad E_{0y} = \sum_{n=1}^{N} b_{j+1,n}, \qquad E_{2x} = \sum_{n=1}^{N} \lambda_n^2 a_{j+1,n}, \qquad E_{2y} = \sum_{n=1}^{N} \lambda_n^2 b_{j+1,n}, \quad (34)$$

$$a_{j+1,n} \geqslant 0, \qquad b_{j+1,n} \geqslant 0, \qquad c_{j+1,n} \geqslant 0, \quad (35)$$

$$a_{j+1,n}\, b_{j,n} + a_{j,n}\, b_{j+1,n} - 2c_{j,n}\, c_{j+1,n} \geqslant a_{j,n}\, b_{j,n} - c_{j,n}^2. \quad (36)$$

This problem, being linear in nature, can be easily solved by using the linear programming method. The iterations are repeated until no significant improvement occurs in the objective function and all the constraints are satisfied within desirable accuracy. The mathematical basis for this method can be found in the book by Jacoby *et al*. [25].

4. NUMERICAL RESULTS AND DISCUSSION

We illustrate the formulation developed in the preceeding sections by considering the nature of the transfer functions $H_1(\omega)$, $H_2(\omega)$ and $H_3(\omega)$ and their relation to the critical

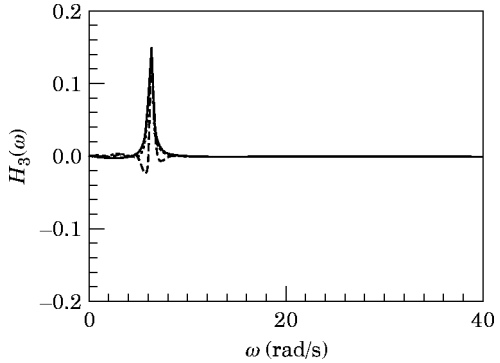

Figure 9. Transfer function H_3 for an sdof system; $\eta = 0{\cdot}05$, $\omega_n = 6{\cdot}1$ rad/s. Time lag (s): —, 0; ·····, 1; ----, 3.

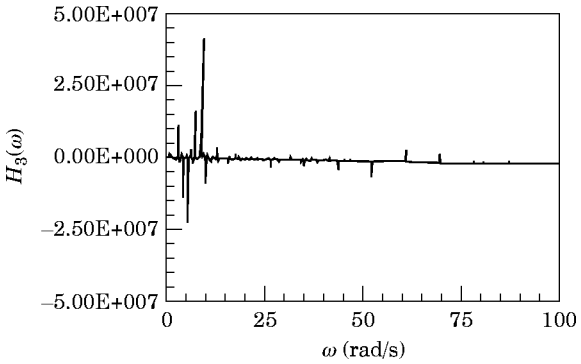

Figure 10. Transfer function H_3 for vertical force transmitted to the left support for the 1620 m span cable with vertical support motions; $\tau = 1$ s.

psd matrix $S(\omega)$ for sdof systems and for a more realistic mdof system; namely, a 1620 m span elastic cable fixed at the two ends, which is typical of a suspended cable of a long span bridge [16]. The cable is assumed to have Young's modulus $E = 8{\cdot}76 \times 10^{10}$ N/m^2, area of cross-section $A = 14{\cdot}5 \times 10^{-4}$ m^2, mass per unit length $\rho = 6{\cdot}35$ kg/m and applied tension $H_0 = 368{\cdot}3$ kN. The role played by the filter function $H_f(\omega)$ in suppressing the singularity in $H_1(\omega)$ at $\omega = 0$ is shown in Figure 3. The variations of $H_1(\omega)$ and $H_2(\omega)$ for sdof systems are shown in Figures 4 and 5, and those for the cable structure are shown in Figures 6 and 7.

In Figures 8(a–c) are shown the features associated with the critical input and response as defined in section 3.1. The variation of g_1 and g_2 in equation (19) for a sdof system is shown in Figure 6(a). A typical critical $\phi_{xy}(\omega)$ in equation (21) is plotted in Figure 6(b). In Figure 6(c) is shown the response psd of the quantity $4F/K$ for different cases of fully coherent excitations: motions in critical-phase (from equation 21 in section 3.1); motions in-phase; motions out-of-phase and independent motions.

Next we consider the special class of problems described in section 3.2. The typical variations of $H_3(\omega, \tau)$ are shown in Figure 9 for a sdof system and Figure 10 for the cable structure. The $S_{xx}(\omega)$ and $S_{yy}(\omega)$ here are taken to be of the form

$$S_0(\omega) = \frac{\phi_0 [1 + 4\zeta_g (\omega/\omega_g)^2]}{[1 - (\omega/\omega_g)^2]^2 + 4\zeta_g^2 (\omega/\omega_g)^2}. \tag{37}$$

It is assumed in the numerical work that for $S_{xx}(\omega)$, $\omega_g = 18{\cdot}8$ rad/s and $\zeta_g = 0{\cdot}60$ and for $S_{yy}(\omega)$, $\omega_g = 31{\cdot}41$ rad/s and $\zeta_g = 0{\cdot}60$, which lead to $E_{0x}/g^2 = 0{\cdot}94$, $E_{0y}/g^2 = 0{\cdot}82$, $n_{0x}^+ = 3{\cdot}0$ Hz and $n_{0y}^+ = 5{\cdot}0$ Hz. The critical cross-psds obtained by using equation (24) in

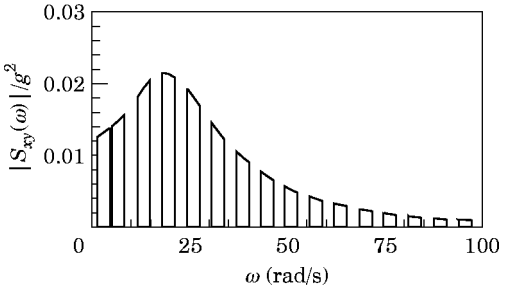

Figure 11. Critical $|S_{xy}(\omega)|$ for sdof system when S_{xx} and S_{yy} are known; $\omega_n = 6{\cdot}1$ rad/s, $\eta = 0{\cdot}05$.

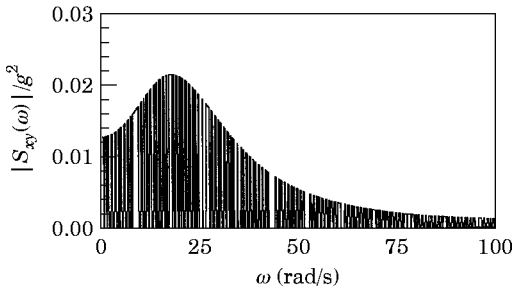

Figure 12. Critical $|S_{xy}(\omega)|$ for the 1620 m cable when S_{xx} and S_{yy} are known; support motions are vertical and response variable is the vertical force transmitted to the support.

section 3.2 are shown for the sdof system in Figure 11 and for the cable structure in Figure 12.

For the more general case discussed in section 3.3, the results obtained on critical psd functions are shown in Figures 13–16. In these results, it is assumed that $E_{0x}/g^2 = 0{\cdot}94$, $E_{0y}/g^2 = 0{\cdot}82$, $n_{0x}^+ = 3{\cdot}0$ Hz, $n_{0y}^+ = 5{\cdot}0$ Hz, $\omega_1 = 1$ rad/s and $\omega_2 = 100$ rad/s. The linear programming at every iteration stage is solved by using the IMSL routine DDLPRS.

From a careful study of the numerical results obtained, the following points emerge.

1. The functions H_1 and H_2 for sdof systems show a maximum near the frequency of the filter function $H_f(\omega)$, that is, near $\omega = \omega_f = 5{\cdot}5$ rad/s and another peak near the system natural frequency. The relative magnitudes of these two peaks play a significant role in deciding the qualitative nature of the critical psd functions. Naturally, one can conceive a specific system for which the two peaks in the transfer function are equal; the natural frequency of this system serving as a transition frequency to demarcate "low" and "high" frequency systems. For the results shown in Figures 4 and 5, this transition frequency is about 17·0 rad/s. For low frequency systems the dominant peak appears at the system natural frequency while for high frequency system the highest peak lies near the filter frequency.

2. For the cable structure studied, the H_1 and H_2 functions given by equation (16) which correspond to the transverse response, clearly show the packing of densely spaced dominantly transverse modes between the more sparsely spaced dominantly longitudinal modes. On the other hand, the function given by equation (17) for the horizontal force transmitted to the support the longitudinal modes dominates.

3. While H_1 and H_2 are non-negative and independent of the time lag parameter τ, the function H_3, on the other hand, depends on τ and can take both positive and negative values. For fixed value of ω, this function is periodic in τ with frequency $\omega/2\pi$. The variations in ω for a given τ is more complicated with rapid variations occurring near the system natural frequencies and filter frequency.

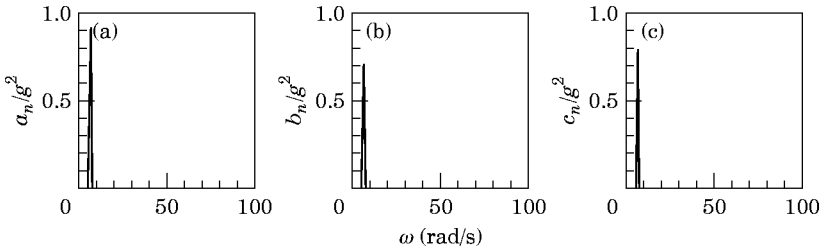

Figure 13. Critical power spectra for sdof system; $\omega_n = 6{\cdot}1$ rad/s, $\eta = 0{\cdot}05$, $\tau = 1$ s, $E_{0x}/g^2 = 0{\cdot}94$, $E_{0y}/g^2 = 0{\cdot}82$. $n_{0x}^+ = 3{\cdot}0$ Hz and $n_{0y}^+ = 5{\cdot}0$ Hz: (a) S_{xx}; (b) S_{yy}; (c) $|S_{xy}|$.

4. While g_2 in equation (19) is always positive, g_1 can have either positive and negative values. In Figure 8(a), the region where pseudo-static component dominates, g_1 is negative while it is positive around the natural frequency of the system, the region where dynamic component dominates. In Figure 8(b) it is shown that the critical phase ϕ_{xy} undergoes a sharp change at the zero of g_1 which demarcates the frequency regions in which pseudo-static and dynamic components dominate. In Figure 8(c) it is shown that in the region where the pseudo-static effect dominates, the critical psd follows the spectrum produced by out-of-phase motions. In the region in which the dynamic effect dominates, the critical psd merges with the spectrum produced by in-phase excitations. However, the fully coherent critical cross-psd from section 3.1 represents neither in-phase nor out-of phase excitations. These critical coherent ground motions have a specific phasing which entirely depends on system parameters.

5. The critical $|S_{xy}(\omega)|$ functions derived as per equation (24) consist of an alternating sequence of frequency windows in which the function takes its extreme admissible values; namely, zero and $\sqrt{S_{xx}(\omega)S_{yy}(\omega)}$, respectively. The spacing of these windows is governed by the zeros of transfer function H_3, which, for a given system, shows significant variations with respect to τ. The overall shape of the cross spectra is observed to be governed by the shape of $S_{xx}(\omega)$ and $S_{yy}(\omega)$; see Figures 11 and 12.

6. The critical psd functions obtained using the iterative linear programming formulation presented in equations (29)–(36) (see Figures 13–16) display strong resonant characteristics with most of the average power concentrated near a single frequency which correspond to the location of highest peak in H_1 and H_2. For low frequency sdof systems, most of the power is concentrated at the system natural frequency, and thus the response is dominated by resonant behavior. On the other hand, for high frequency sdof systems, power is concentrated near the filter frequency ω_f, with the exact location being at the point near ω_f at which H_3 has the highest positive peak. The critical $\ddot{x}(t)$ and $\ddot{y}(t)$ here are fully coherent if $H_3(\omega, \tau)$ is positive at the frequency at which S_{xx} and S_{yy} peak; otherwise, they are incoherent. Thus, for a given system, the critical $\ddot{x}(t)$ and $\ddot{y}(t)$ could be either fully coherent or incoherent depending on value of τ.

7. For the cable structure, the critical psd functions shown in Figures 15 and 16 again show a highly narrow-banded nature, notwithstanding the fact that the system has densely spaced modes. The frequency at which the power is concentrated again depends upon the point at which the transfer functions H_1 and H_2 have the highest peak and whether H_3 is positive at this frequency. For the two cases considered this frequency is observed to lie close to the frequency of the first dominant longitudinal mode.

8. In the critical psd functions shown in Figures 13–16, the constraints on the zero crossing rates n_{0x}^+ and n_{0y}^+ are satisfied through the presence of a barely perceptible peak at the higher end of frequency range; namely, at $\omega_2 = 100$ rad/s, with no peak appearing in the psd function at the dominant ground frequency as one might intuitively expect.

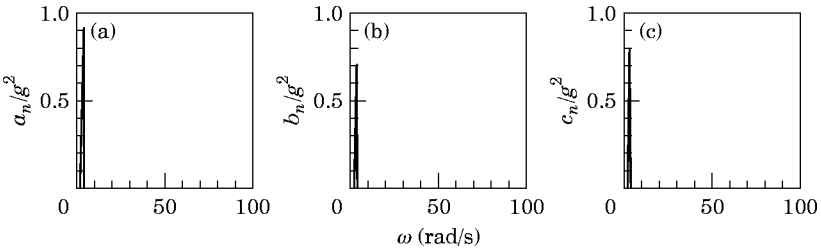

Figure 14. Critical power spectra for sdof system; $\omega_n = 25{\cdot}1$ rad/s, $\eta = 0{\cdot}05$, $\tau = 1$ s, $E_{0x}/g^2 = 0{\cdot}94$, $E_{0y}/g^2 = 0{\cdot}82$, $n_{0x}^+ = 3{\cdot}0$ and $n_{0y}^+ = 5{\cdot}0$ Hz; (a) S_{xx}; (b) S_{yy}; (c) $|S_{xy}|$.

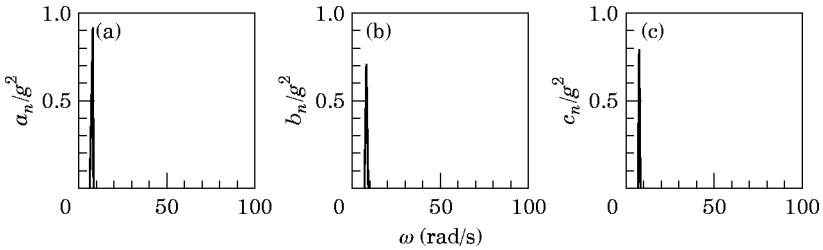

Figure 15. Critical power spectra for 1620 m span cable; $\tau = 1$ s, $E_{0x}/g^2 = 0{\cdot}94$, $E_{0y}/g^2 = 0{\cdot}82$, $n_{0x}^+ = 3{\cdot}0$ Hz and $n_{0y}^+ = 5{\cdot}0$ Hz; support motions are vertical and response variable is the vertical force transmitted to the support: (a) S_{xx}; (b) S_{yy}; (c) $|S_{xy}|$.

9. The critical response obtained for the different systems considered is shown in Table 1. As might be expected, for a given system, the critical response is the highest when the prior information on the input is the least. Thus, the response obtained with the critical-psd model of equation (24), in which knowledge of S_{xx} and S_{yy} is assumed, is always less than the results given by using the linear programming formulations of equations (29–36), in which constraints are imposed only on the spectral moments of S_{xx} and S_{yy}.

10. The critical response shows an interesting dependence on the time lag τ; see Figure 17. The response at $\tau = 0$ represents one of the maxima for low frequency systems, while for high frequency systems it represents a minimum. The lowest responses in this figure were observed to occur when $\ddot{x}$ and $\ddot{y}$ were incoherent. For mdof systems the variation of critical response with τ showed a fairly complicated structure with no easily discernible features.

11. The optimization iterations were generally observed to converge within about four to five cycles of iterations. No matter how the solution was started, the same optimal solutions were obtained. This is illustrated in Figure 18, in which the critical responses at different stages of iterations for three different starting solutions are shown. It may be observed that one of the sequence of solutions produces an intermediate response higher than the eventual optimal solution. However, it must be noted that the intermediate higher responses are not produced by feasible solutions: that is, even though the iterations were initiated with a feasible solution, the intermediate solutions exited the feasible region temporarily, this in turn arising due to the approximate manner in which the non-linear constraint (32) is satisfied at every iteration.

5. ENTROPY RATE AS A MEASURE OF DISORDER IN CRITICAL EXCITATIONS

The critical psd models developed by using the iterative linear programming scheme outlined in section 3.3 indeed lead to the determination of the highest response possible

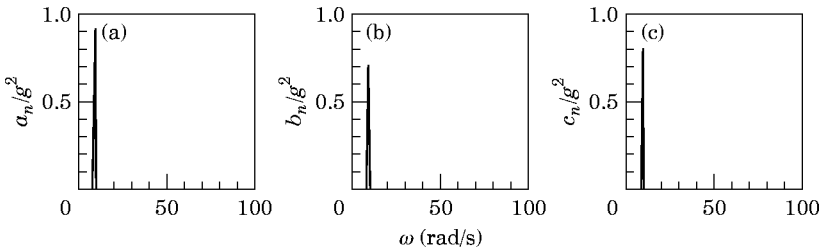

Figure 16. Critical power spectra for 1620 m span cable; $\tau = 1$ s, $E_{0x}/g^2 = 0{\cdot}94$, $E_{0y}/g^2 = 0{\cdot}82$, $n_{0x}^+ = 3{\cdot}0$ Hz and $n_{0y}^+ = 5{\cdot}0$ Hz; support motions are horizontal and response variable is the horizontal force transmitted to the support: (a) S_{xx}; (b) S_{yy}; (c) $|S_{xy}|$.

TABLE 1

Stationary response standard deviation of different systems

No.	Basis of solution	$\sqrt{\sigma^2/g^2}$ Case A s^2	Case B s^2	Case C kN m^{-1} s^2	Case D kN m^{-1} s^2
1	As in section 3.2, S_{xx} and S_{yy} as in equation (37)	0·044	0·014	0·604	17·71
2	As in section 3.3, $E_{0x}/g^2 = 0{\cdot}94$, $E_{0y}/g^2 = 0{\cdot}82$, $n_{0x}^+ = 3{\cdot}0$ Hz, $n_{0y}^+ = 5{\cdot}0$ Hz	0·472	0·070	5·901	70·68
3	As in section 5, $E_{0x}/g^2 = 0{\cdot}94$, $E_{0y}/g^2 = 0{\cdot}82$, $n_{0x}^+ = 3{\cdot}0$ Hz, $n_{0y}^+ = 5{\cdot}0$ Hz, $M = 12$	0·296	0·041	3·570	44·30
4	S_{xx} and S_{xx} as per equation (37); $\ddot{x}$ and $\ddot{y}$ fully incoherent	0·034	0·012	0·514	12·74
5	S_{xx} and S_{xx} as per equation (37); $\ddot{x}$ and $\ddot{y}$ fully coherent	0·043	0·012	0·552	16·95

Case A: sdof system; $\omega_n = 6{\cdot}1$ rad/s; $\eta = 0{\cdot}05$; $\tau = 1$ s.
Case B: sdof system; $\omega_n = 25{\cdot}1$ rad/s; $\eta = 0{\cdot}05$; $\tau = 1$ s.
Case C: cable structure; $\tau = 1$ s; support motions are vertical and response variable is the vertical force transmitted to the left support.
Case D: cable structure; $\tau = 1$ s; support motions are horizontal and response variable is the horizontal force transmitted to the left support.

under the action of partially specified excitations; however, they fail to be acceptable models for possible earthquake excitations because of their nearly deterministic nature. This points towards the fact that the prior knowledge of earthquake records as being random in nature has not been made total use of in defining critical excitations. The question thus would arise as how to *quantify* this prior knowledge and incorporate it into the definition of critical excitations. Such a measure can be included into the framework of critical excitation modelling either by modifying the objectives or by imposing new constraints. It is expected out of such an exercise that it enforces redistribution of seismic energy to frequencies other than those associated with the structure or the singularity suppressing filter functions. This, of course, would bring down the magnitude of structural damage but would make the critical seismic excitations more realistic.

In this context, it may be noted that the principle of maximum entropy has been widely used in stochastic modeling in science in engineering; see, for example, the comprehensive monograph on this topic by Kapur [26]. This principle provides a powerful means to handle problems involving incompletely specified probability space. Given that the concept of random critical excitation primarily deals with incompletely specified random processes, it is of interest to explore the relevance of entropy rate considerations in defining critical excitations. Thus it would be of interest to define critical excitations which satisfy an additional constraint that they possess entropy rates which are commensurate with those associated with accepted models for earthquake excitations. Motivated by this consideration, the present authors have recently examined the consequences of incorporating entropy rate considerations in characterizing the critical psd functions for single point excitations [11]. A feature which was observed during this study was that excitations with higher entropy rates produce lower responses. We reiterate here the

arguments used in our previous paper but set them in the context of multiple support excitations.

We begin by considering the proposal that the definition of random critical excitations be modified to incorporate an additional objective that the excitations not only maximize system response but also produce the highest entropy rate consistent with the partial information available: the aim being to produce optimally disordered critical excitations. Briefly stated, the problem now consists of finding the input psd matrix which would not only maximize the response variance given by equation (7) under the constraints of equations (25) and (26), but also, maximize the entropy rates of the processes $\ddot{x}(t)$ and $\ddot{y}(t)$ given, respectively, by

$$\bar{H}_x = \log_e \sqrt{2\pi e} + \frac{1}{2(\omega_2 - \omega_1)} \int_{\omega_1}^{\omega_2} \log_e S_{xx}(\omega)\, d\omega \tag{38}$$

and

$$\bar{H}_y = \log_e \sqrt{2\pi e} + \frac{1}{2(\omega_2 - \omega_1)} \int_{\omega_1}^{\omega_2} \log_e S_{yy}(\omega)\, d\omega \tag{39}$$

It may be noted that this definition of entropy rate assumes that the random processes $\ddot{x}$ and $\ddot{y}$ are Gaussian [27]. Now the problem not only has multiple objectives but, also, additional non-linearities have been introduced through the new objective functions. One way in which to solve this problem is to maximize separately the functions $\bar{H}_x$ and $\bar{H}_y$ under the constraints of equation (25) and (26) and subsequently impose the resulting maximum entropy rates as additional constraints in maximizing the response variance. The first level of optimization can be carried out within the framework of calculus of variations in conjunction with Lagrangian multipliers. This consists of, for example, finding the maximum of the Lagrangian

$$L_x(S_{xx}, \nu_1, \nu_2) = \log_e \sqrt{2\pi e} + \frac{1}{2(\omega_2 - \omega_1)} \int_{\omega_1}^{\omega_2} \log_e S_{xx}(\omega)\, d\omega$$

$$+ \nu_1 \left[-E_{0x} + \int_{\omega_1}^{\omega_2} S_{xx}(\omega)\, d\omega \right] + \nu_2 \left[-E_{2x} + \int_{\omega_1}^{\omega_2} \omega^2 S_{xx}(\omega)\, d\omega \right], \tag{40}$$

where ν_1 and ν_2 are Lagrangian multipliers. This leads to the maximum entropy psd function

$$\tilde{S}_{xx}(\omega) = -2(\omega_2 - \omega_1)/(\nu_1 + \omega^2 \nu_2), \tag{41}$$

from which one can find the maximum entropy $\bar{H}_x^*$. By using a similar procedure, $\bar{H}_y^*$ can also be determined. The next step is to maximize σ^2 under the constraints of equations (25) and (26) and the additional constraints

$$\bar{H}_x^* = \log_e \sqrt{2\pi e} + \frac{1}{2(\omega_2 - \omega_1)} \int_{\omega_1}^{\omega_2} \log_e S_{xx}(\omega)\, d\omega \tag{42}$$

and

$$\bar{H}_y^* = \log_e \sqrt{2\pi e} + \frac{1}{2(\omega_2 - \omega_1)} \int_{\omega_1}^{\omega_2} \log_e S_{yy}(\omega)\, d\omega \tag{43}$$

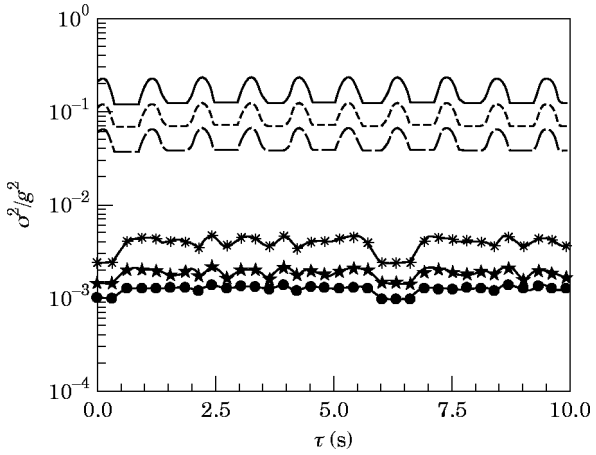

Figure 17. Critical response for sdof system; $\eta = 0{\cdot}05$. Natural frequency (rad/s), M: —, 6·1, 1; ----, 6·1, 5; — —, 6·1, 12, ∗—∗, 25·1, 1; ★—★, 25·1, 5; ●—●, 25·1, 12.

The previous studies which we have carried out on single point excitations [11] have shown that this approach has the following two drawbacks.

(a) The approach results in very low response levels, which is indicative of loss of sense of criticality. In fact, the response obtained was found to be lower than what would be produced by a Kanai–Tajimi earthquake model with comparable variance zero crossing rate.

(b) The resulting input entropy rates were much higher that those associated with valid earthquake random process models such as the Kanai–Tajimi stationary random process model.

To circumvent these difficulties two measures were considered.

(a) Define a utility function which is a weighted sum of system response and the input entropy rate and find the optimal psd function which maximize the utility function.

(b) Relax the maximum entropy constraint by requiring that the critical psd functions need not have the highest entropy rate as imposed above but, instead, resemble the maximum entropy psd functions $\tilde{S}_{xx}(\omega)$ and $\tilde{S}_{yy}(\omega)$ only partially. This can be achieved by calculating the spectral moments of $\tilde{S}_{xx}(\omega)$ and $\tilde{S}_{yy}(\omega)$ and impose them as additional constraints in maximizing the response variance.

Of these two options, the last option was found to be feasible from the point of view of implementation. In the present problem, this latter option has the advantage that the

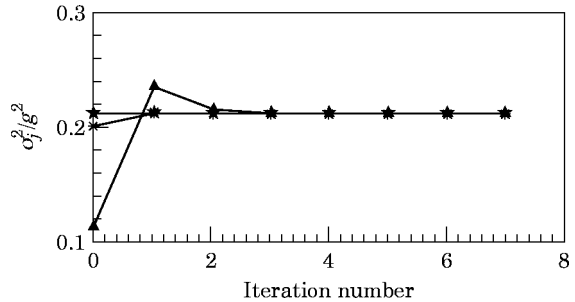

Figure 18. Convergence of critical response for sdof system with different feasible starting solutions; $\eta = 0{\cdot}05$; $\omega_n = 6{\cdot}1$ rad/s. Starting solution: ∗—∗, 1; ★—★, 2; ▲—▲, 3.

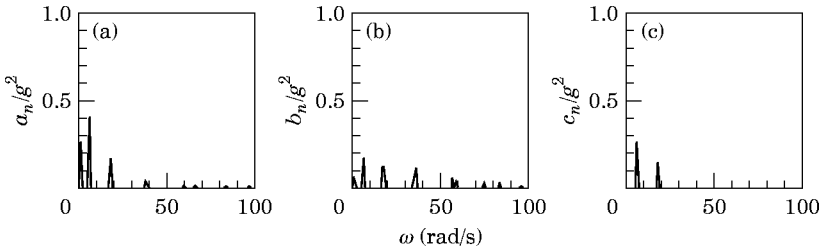

Figure 19. Critical power spectra for an sdof system with entropy rate constraints; $\omega_n = 6{\cdot}1$ rad/s, $\eta = 0{\cdot}05$, $\tau = 1$ s, $E_{0x}/g^2 = 0{\cdot}94$, $E_{0y}/g^2 = 0{\cdot}82$, $n_{0x}^+ = 3{\cdot}0$ Hz and $n_{0y}^+ = 5{\cdot}0$ Hz and $M = 12$: (a) S_{xx}; (b) S_{yy}; (c) $|S_{xy}|$.

resulting problem can be solved within the framework of the iterative linear programming method outlined in section 3.3. Thus, it is required to maximize the system response given by equation (7) under the constraints (25) and (26) and the additional spectral moment constraints given by

$$\int_{\omega_1}^{\omega_2} \omega^k \tilde{S}_{xx}(\omega)\,\mathrm{d}\omega = \int_{\omega_1}^{\omega_2} \omega^k S_{xx}(\omega)\,\mathrm{d}\omega, \tag{44}$$

$$\int_{\omega_1}^{\omega_2} \omega^k \tilde{S}_{yy}(\omega)\,\mathrm{d}\omega = \int_{\omega_1}^{\omega_2} \omega^k S_{yy}(\omega)\,\mathrm{d}\omega, \qquad k = 0, 1, 2, \ldots, M. \tag{45}$$

The resulting critical psd functions are now functions of the number of spectral moment constraints imposed. An important feature which has been observed in our studies is that with the increases in the value of M, the entropy rate increases monotonically and the response on the other hand is reduced monotonically [11]. This would mean that, the parameter M can be used to control the level of disorder that might be expected in the critical excitation.

In Figures 19 and 20 are shown the critical psd obtained by using the above formulation with $M = 12$ for the sdof and the cable structures studied previously. The critical response variance obtained is listed in Table 1. The consideration of entropy rate as a measure of uncertainty has been observed to bring down the critical response (see Figure 17) and make the critical excitations rich in frequency content. In Figure 21 are shown Gaussian samples of critical excitations generated compatible with the psd shown in Figure 20, which corroborate the latter observation. As has been already noted, the critical psd and the response are now dependent on M and, consequently, the question of choosing M becomes

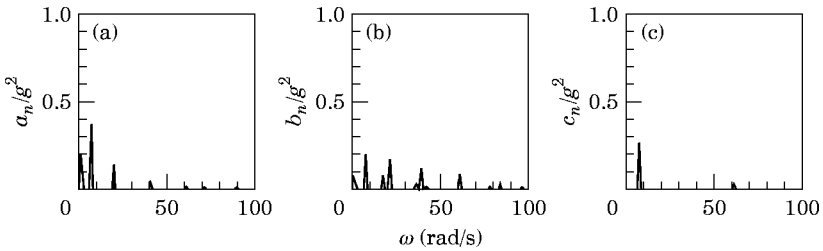

Figure 20. Critical power spectra for 1620 m cable with entropy rate constraints; $\tau = 1$ s, $E_{0x}/g^2 = 0{\cdot}94$, $E_{0y}/g^2 = 0{\cdot}82$, $n_{0x}^+ = 3{\cdot}0$ Hz and $n_{0y}^+ = 5{\cdot}0$ Hz and $M = 12$; support motions are vertical and response variable is the vertical force transmitted to the support: (a) S_{xx}; (b) S_{yy}; (c) $|S_{xy}|$.

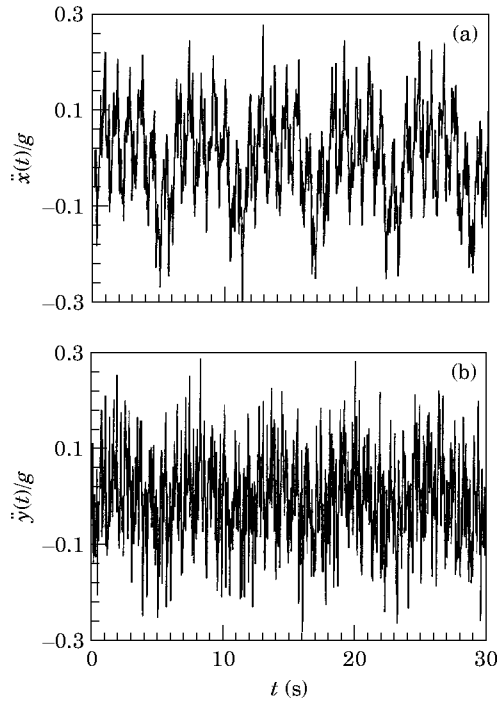

Figure 21. Sample critical excitations compatible with psd functions of Figures 22 and 23 with $E_{0x} = 9.4 \times 10^{-3}\, g^2$ and $E_{0y} = 8.2 \times 10^{-3}\, g^2$: (a) $\ddot{x}$ for 1620 m span cable; (b) $\ddot{y}$ for 1620 m span cable.

important. This requires further studies on entropy rate as a descriptor of disorder in random process models for earthquake loads.

6. CONCLUSIONS

Specification of the seismic inputs with account taken of their multi-component and spatial variability effects requires the characterization of the input as a vector of excitations. This characterization must encapsulate not only the time and frequency characteristics of individual components, but also, the cross-correlations among the distinct components. Design methods employing the traditional response spectrum philosophy are at a disadvantage in this context. This is because, the response spectra, by definition, deal only with a single excitation component. The concept of critical cross-power spectral density functions, developed in this paper, aims to establish the optimal cross-correlation amongst the distinct excitation components, which, in turn, leads to the highest response in a given structure, and provides a counterpoint in multi-components/multi-support earthquake input modelling.

This paper introduces the definition of critical seismic psd matrices for extended structures supported discretely at two points and outlines an iterative optimization procedure based on linear programming method for the determination of the critical psd functions. These functions produce highest steady state response variance in a given linear structure and at the same time satisfy constraints on variance, average zero crossing rates, frequency content and transmission time lag. The usefulness of imposing constraint in terms of entropy rate as a quantitative measure of uncertainty is also discussed. In the special case in which knowledge of auto-spectral densities is available, the critical

cross-spectral density function represents fully coherent motions which are produced by neither in-phase nor out-of-phase support motions. This model of critical excitations can be useful to study the critical response of short-span stiff structures based on rapidly varying local soil conditions. In this case, the main source of spatial variability of the ground motions is due to the site-response effect, which can be modelled by the phase spectrum alone. Moreover, this model can be used to obtain the *exact* upper bounds of response of multiply supported secondary systems such as piping networks in nuclear industry. The upper bounds of the response obtained can be utilized to study the validity of the existing design practice. In the other case where, in addition to the knowledge of auto-spectral densities, the phase spectrum of excitations is also taken to be known, the critical response is produced by a specific form of coherent motions which represents neither fully coherent nor fully incoherent ground motions. This model of excitations is suitable for long-span structures where the variability of the ground motions is primarily influenced by coherency loss and wave-passage effects. Extension of the approach discussed here is to include nonstationary random excitations and to develop random field excitation models is currently being studied by the present authors.

ACKNOWLEDGMENTS

The work reported in this paper has been carried out as a part of a research project on dynamics of extensible cables funded by the Department of Science and Technology, Government of India. The financial support received is gratefully acknowledged.

REFERENCES

1. N. C. Nigam and S. Narayanan 1994 *Applications of Random Vibrations*. New Delhi: Narosa.
2. R. F. Drenick 1970 *Journal of Engineering Mechanics* **96**, 483–493. Model-free design of aseismic structures.
3. R. F. Drenick 1973 *Journal of Engineering Mechanics* **99**, 649–667. Aseismic design by way of critical excitations.
4. A. A. Pirasteh, J. L. Cherry and R. J. Balling 1988 *Earthquake Engineering and Structural Dynamics* **16**, 597–613. The use of optimization to construct critical accelerograms for given structures and sites.
5. M. Srinivasan, B. Ellingwood and R. Corotis 1991 *Journal of Engineering Mechanics* **117**, 1403–1422. Critical base excitations of structural systems.
6. P. C. Wang, R. D. Drenick and W. Y. L. Wang 1978 *Journal of Engineering Mechanics* **104**, 441–456. Seismic assessment of high-rise buildings.
7. R. N. Iyengar 1989 *Proceedings of the 5th ICOSSAR*, *San Francisco*; New York: ASCE Publications. Critical seismic excitation for structures.
8. P. C. Wang and C. B. Yun 1979 *Earthquake Engineering and Structural Dynamics* **7**, 569–578. Site-dependent critical design spectra.
9. R. N. Iyengar 1970 *Report* 47 *series J; Center of Applied Stochastics*, *Purdue University*, *West Lafayette*, *Indiana*. 1970. Matched inputs.
10. R. N. Iyengar, C. S. Manohar 1987 *Journal of Engineering Mechanics* **133**, 529–541. Nonstationary random critical seismic excitations.
11. C. S. Manohar and A. Sarkar 1995 *Earthquake Engineering and Structural Dynamics* **24**, 1549–1566. Critical earthquake input power spectral density models for engineering structures.
12. M. Srinivasan, R. Corotis and B. Ellingwood 1992 *Earthquake Engineering and Structural Dynamics* **21**, 275–288. Generation of critical stochastic earthquakes.
13. H. Hao 1993 *Earthquake Engineering and Structural Dynamics* **22**, 389–404. Arch response to correlated multiple excitations.

14. R. S. Harichandran and W. Wang 1990 *Earthquake Engineering and Structural Dynamics* **19**, 173–187. Response of indeterminate two-span beam to spatially varying seismic excitation.
15. A. S. Nazmy and A. M. Abdel-Ghaffar 1992 *Earthquake Engineering and Structural Dynamics* **21**, 1–20. Effects of ground motion spatial variability on the response of cable-stayed bridges.
16. G. V. Rao 1989 *PhD. Thesis*, *Department of Civil Engineering*, *Indian Institute of Science*. Vibration of cables under deterministic and random excitations.
17. A. Zerva, A. H. S. Ang, and Y. K. Wen 1988 *Earthquake Engineering and Structural Dynamics* **16**, 361–379. Lifeline response to spatially variable ground motions.
18. A. Zerva 1991 *Probabilistic Engineering Mechanics* **6**, 212–221. Effect of spatial variability and propagation of seismic ground motions on the response of multiply supported structures.
19. B. A. Bolt, C. H. Loh, J. Penzien, Y. B. Tsai and Y. T. Yeh 1982 *Earthquake Engineering and Structural Dynamics* **10**, 561–573. Earthquake strong motions recorded by a large near source array of digital seismographs.
20. R. S. Harichandran and E. Vanmarcke 1986 *Journal of Engineering Mechanics*, *American Society of Civil Engineers* **112**, 154–174. Stochastic variations of earthquake ground motion in space and time.
21. N. A. Abrahamson, J. F. Schneider and J. C. Stepp 1991 *Earthquake Spectra* **7**, 1–28. Empirical spatial coherency functions for application to soil–structure interaction analysis.
22. A. Der Kiureghian 1996 *Earthquake Engineering and Structural Dynamics* **25**, 99–111. A coherency model for spatially varying ground motions.
23. P. Banerjee 1994 *Current Science* **67**, 386–394. Earthquake ground motion characterization for large or multiply supported structures.
24. R. H. Clough and J. Penzien 1975 *Dynamics of structures*. Tokyo: McGraw-Hill Kogakusha.
25. S. L. S. Jacoby, J. S. Kowalik and J. T. Pizzo 1972 *Iterative Methods for Nonlinear Optimization Problems*. Englewood Cliffs, New Jersey: Prentice Hall.
26. J. N. Kapur 1993 *Maximum Entropy models in Science and Engineering*. New Delhi: Wiley Eastern.
27. A. Papoulis 1991 *Probability*, *Random Variable and Stochastic Processes*. New York: McGraw-Hill.
28. A. Sarkar and C. S. Manohar 1996 *Archives of Applied Mechanics* **66**, 315–325. Dynamic stiffness matrix of a general cable element.
29. A. Sarkar and C. S. Manohar 1996 *Earthquake Engineering and Structural Dynamics* **25**, 303–315. Critical cross power spectral density functions and the highest response of multi-supported structures subjected to multi-component earthquake excitations.
30. M. P. Singh, R. A. Burdisso and G. O. Maldonado 1992 *Transactions of the American Society of Mechanical Engineers*, *Journal of Pressure Vessel Technology* **114**, 46–52. Methods used for calculating seismic response of multiply supported piping systems.